Monterey Excursion Events in the Middle Miocene Carbonate Rock Succession, Eastern Iraq

Mustafa A. Ali
Iraq Geological Survey
Sa'ad Z. Al-Mashaikie
University of Baghdad
Arsalan Ahmed Othman (arsalan.aljaf@gmail.com)
Iraq Geological Survey https://orcid.org/0000-0002-4212-228X

Research Article

Keywords: Stable isotope, Jeribe Formation, Monterey excursion, Miocene, Palaeoceanography

Posted Date: April 12th, 2021

DOI: https://doi.org/10.21203/rs.3.rs-369744/v1

Abstract

The global Monterey excursions are recognized in many deep-sea, and recently in shallow water depth records during the Miocene epoch. We analyzed the δ 13C and δ 18O to investigate the relationship between the lithostratigraphic units and the deviation of the stable isotopes. The results show that there is a significant relationship between the depositional energy changes and both of δ 13C and δ 18O. The present paper is deals with variability of the primary isotopic composition of seawater in the shallow water zone. Sedimentary successions of middle Miocene outcropping in the eastern part of Iraq provide an excellent archive of the oxygen isotope events (Mi-events), additional details about Mi 2 and Mi 3 zones of glaciations and refine the Monterey Excursion, carbonate isotope maxima (CM-events). Facies analysis revealed several microfacies could be distinguished, reflecting depositional environments including; lagoon, back reef-reef, shallow open marine, and shoal environments. The Jeribe Formation is a transgression unit belonging to the stage Ap11 tectonostratigraphy Megasequence. The Formation was deposited in the outer platform margin of unstable shelf of the Arabian Plate and significant of this formation, which is deposited during the final phase of Tethys sea closure. The stable isotope (18O/16O and 13C/12C) provide an excellent archive of the paleoceanography for the Neogene (middle Miocene Transgression) of the Neo-Teythys. Oxygen and carbon isotopic stratigraphy for bulk-rock were analyzed in order to distinguished Monterey Event and climate optima.

1. Introduction

The Monterey excursions are large disturbance with a $\delta^{13}C$ shift toward heavier values. Woodruff & Savin (1991) were the first researchers who recorded the Monterey excursions events and recognized the variation of the internal periodic in the $\delta^{13}C$. They defined six so-called carbon isotope maxima (CM-events). The Shift of $\delta^{13}C$ to heavier values is recognised in many deep-sea locations. Recently, it has been recorded during Miocene at ~ 17.5 Ma, terminating at ~ 13.5 Ma in shallow water depth (Vincent and Berger 1985; Corfield and Cartlidge 1993; Flower and Kennett 1993, 1994, 1995; Smart and Murray 1994; Rea et al. 1998; Mourik et al. 2010; Auer et al. 2015). Isotopic studies on the shallow marine carbonates of the Miocene have revealed evidence for paleo-tectonic (Kumar et al. 2002; Madhavaraju et al. 2004; Maheshwari et al. 2005; Marquillas et al. 2007; Nagarajan et al. 2008; Armstrong-Altrin et al. 2009) and global scale tectonic events (Gröcke et al. 2005; Maheshwari et al. 2005; Amodio et al. 2008).

The Monterey Formation in California shows dramatic increases in organic carbon accumulation in Pacific Rim sediments linked to invigorated coastal and equatorial upwelling of high carbon and oxygen content (Vincent and Berger 1985; Woodruff and Savin 1991). The significant positive carbon isotope shift is generally used to establish the global organic carbon budget during the oceanic anoxic events. Scholle & Arthur (1980) suggested that the volume of organic carbon (C_{org}) buried was a sizable part of the global carbon budget.

Miller and Katz (1987), Flower and Kennett (1994), Zachos et al. (2001), Billups and Schrag (2003), Holbourn et al. (2007), James *et al.* (2008), and Diester-Haass et al. (2013) considered the major climatic

shift during the Neogene is marking for the beginning of the gradual transition from the middle Miocene into the icehouse climate of the Pleistocene. Miller and Katz (1987), Diester-Haass *et al.* (2013), and Billups and Schrag (2003) used the benthic foraminiferal accumulation from Deep Sea Drilling Project in different sites, Hole 588 in the Pacific and Southern Oceans, Sites 558 and 563 in North Atlantic, and 757 and 689 from the subtropical Indian Ocean and the Weddell Sea, respectively, showed a distinct productivity maximum during CMs and link their occurrences to the time of major expansion of ice on Antarctica. Woodruff and Savin (1991) stated similar conclusion about the carbon isotope maxima recorded by in Ocean Drilling Program Site 747. Comparable events were also recorded for oxygen isotope data during the Miocene (Chaproniere 1981; Cooke et al. 2008; Diester-Haass et al. 2013; Auer et al. 2015).

The Miocene oxygen isotope events (Mi-1–Mi-7) were noticed to be globally concurrent and are related to the change of paleo-climate. These event were named by Scott, Nelson and Stone (1995) as glacial zones indicating global cooling. Miller *et al.* (1991), Miller *et al.* (1991); Wright et al. (1992), Westerhold et al. (2005), and Chakrabarti et al. (2011) described a number of extreme glacial events from $\delta^{18}O$ records, called Mi zones and linked Mi1to Mi4 zones to the east Antarctic ice sheet expansion, while Mi5, Mi6, and Mi7 zones were associated with the ice volume accumulation on the western part of Antarctica through the middle-late Miocene. Cooling or glacial prominent period occurs synchronously with CM events (Sosdian et al., 2020 and refernce in there).

Numerous of published studies stated that the positive relation indicates a global $\delta\ ^{13}C$ excursion are coincides with $\delta^{18}O$ increases value, which are more significance in cool deep water. Sosdian et al. (2020) proposed, for coincidentally, that these events are associated with elevated oceanic dissolved inorganic carbon caused by volcanic degassing and organic carbon burial caused by sea-level rise on drowned continental shelves. He has documented a positive carbon isotope excursion ($\delta^{13}C$) of the global ocean's records in planktonic and benthic foraminifera. Moreover, these events have been documented in carbonates by Auer et al. (2015) as evidenced by plankton-rich in Mi3a and Mi3b reflect increases of upwelling induced nutrient availability, Mi2a is dominant in siliceous plankton and sponges records, while Mi2b coincide with phosphate hardground records.

Edgar et al. (2015) linked enrichment of heavy carbon in the surface waters to the high productive of photic zone would preferentially remove ^{12}C by photo symbionts and phytoplankton, leaving the ambient seawater enriched in ^{13}C. While below the photic zone, values of the ^{12}C are increased relative to surface waters as a function of reducing photosynthetic activity and re-mineralization of ^{12}C. Raymo et al. (1988) and Ruddiman et al. (1997) linked the enrichment of heavy carbon to chemical weathering from continental arc. Overall, these documents, as evidenced by deep-living benthic foraminifera, reflect slope setting and recorded higher $\delta\ ^{18}O$ values due to cooler basinal water masses and for open ocean shallow-dwelling planktonic species, which is enrichment in ^{13}C by up to 4‰ compared to other setting. According to Immenhauser et al. (2002), water masses down to about 150 m depth documented

isotopically light meteoric water ^{18}O in the modern surface sediments of Great Bahama Bank. Swart and Eberli (2005) mentioned to the absence of variations in $\delta^{13}C$ irrespective of change of facies type.

In the current study, we are shown values variability composition of ^{13}C and ^{18}O respect to their differenced over facies change. Due to severely limit the interpretation of the stable-isotope record of shallow water carbonates, the main objective of this study was to examine the variability of the primary isotopic composition of seawater in this setting.

2. Review Of Geology And Stratigraphy

Bellen et al. (1959) described the Jeribe Formation (Middle Miocene) for the first time from the type locality that comprised 173m thick rock sequence in the Sinjar anticline. The Middle Miocene Jeribe Formation belongs to tectonostratigraphy Megasequence A11, which involves several formations (Fig. 1). It considers as a new transgressive stage in the foredeep shelf margin (Jassim and Goff 2006). The formation was controlled by "Savian" continental collision movement between Arabian and Eurasian plates affecting the foreland basin (Numan 1997; Jassim and Goff 2006). Jeribe Formation was deposited in two main basins, i.e., Mosul and Kirkuk blocks (Jassim and Goff 2006). Aqrawi et al. (2010) described the Miocene sequence, microfacies, and depositional environment of the Jeribe Formation. Fouad (2012) stated that the Jeribe Formation was deposited in the outer platform margin.

Stable isotopes of $\delta^{13}C$ and $\delta^{18}O$ of the Jeribe carbonates were recorded for the first time by Ali & Sa'ad (2018a). They concluded variation composition on both $\delta^{13}C$ and $\delta^{18}O$ were controlled by sea-level oscillation. Depletion of $\delta\ ^{13}C$ and $\delta\ ^{18}O$ isotopes are controlled by lowering the sea-level in restricted to shallow marine facies, and *verse versa*, the enrichment of $\delta\ ^{13}C$ and $\delta\ ^{18}O$ isotopes is controlled by sea-level rise. Furthermore, they identified the paleo-depth involve mixed layer and thermocline layer inference by enrichment and depletion of the stable isotopes. Jeribe Formation represents the last deposited marine sediments before the final closure of the southern new Tethys Sea.

3. Methods And Materials

Detailed geological mapping of the study area was preceded by recovering two sections (Figs. 2 and 3). For each section, field description was carried out, such as bed thickness, facies, sedimentary structures, and facies successions. Forty-two samples (at 2–3 m intervals) were collected from fresh surfaces of carbonate rocks, avoiding the late-diagenetic, cracks, veins, weathered materials, and stylolites. Samples were cut perpendicular to the bedding plane to define the textures and mineralogical compositions and obtain the primary signature of isotopes based on the well-preserved texture (Fig. 4). The first section (Ja) is located in the SW core flank of the Koolic-1 anticline, while the second section (Jb) is located in the core of the Koolic-3 anticline in Showshareen valley. The selected sections represent an ideal column of the Kirkuk-Dezful Embayment. Twenty samples were analyzed to determine the stable isotopes of C 12–13 and O18-16 using acid conversion and IRMS. The instrument is a continuous Flow-Isotope Ratio Mass

Spectrometry (CF-IRMS). Analyses were performed in the labs of Iso-Analytical Limited, United Kingdom. A modified version of Hudson's plots reproduced by Nelson and Smith (1996) has been used.

3.1. Carbon-13 and Oxygen-18 Isotopes Analysis

Isotope analysis carried by first adding phosphoric acid to the samples in Clean Exetainer™ tubes after flushing with 99.9% helium for 3 hours at 90°C and allowing it to settle overnight to complete conversion of carbonate to CO_2. Reference and control materials were prepared in the same way. The liberated CO_2 gas was analyzed by Continuous Flow-Isotope Ratio Mass Spectrometry (CF-IRMS). Carbon dioxide was collected in Exetainer™ tubes into a continuously flowing streamed using a double holed needle. The CO_2 was resolved on a packed column gas chromatograph, which is carried forward into the ion source of a Europa Scientific 20–20 IRMS to ionize and accelerate. Gas isotopes of different masses were separated in a magnetic field and simultaneously measured using a Faraday cup collector array to measure the isotopomers of CO_2 at m/z 44, 45, and 46. The phosphoric acid used for digestion had been prepared for isotopic analysis following in accordance with Coplen et al. (1983).

1. Reference Standards and Quality Control

The reference materials used for sample analyses were IA-R022 (Iso-Analytical working standard calcium carbonate, $\delta^{13}C_{V-PDB}$ = -28.63‰ and $\delta^{18}O_{V-PDB}$ = -22.69‰), NBS-18 (carbonatite, $\delta^{13}C_{V-PDB}$ = -5.01‰ and $\delta^{18}O_{V-PDB}$ = -23.20‰), IA-R066 (chalk, $\delta^{13}C_{V-PDB}$ = + 2.33‰ and $\delta^{18}O_{V-PDB}$ = -1.52‰), and quality control. IA-R040 was used as an additional control. The dolomite powder has long-term mean scale corrected values for heavier (carbon 13 and oxygen 18), that have been documented over several years. The measured values for the check samples are provided in the results file. Acid preparations of samples and controls are measured directly against acid preparations of working calcium carbonate standard. This procedure eliminates separate corrections for temperature-dependent isotope fractionation. The results obtained for the NBS-18 and IA-R066 controls are used to check and correct data as required. IA-R022 has been calibrated against and is traceable to NBS-18 and NBS-19 (limestone, $\delta^{13}C_{V-PDB}$ = + 1.95‰, and $\delta^{18}O_{V-PDB}$ = -2.2‰). IA-R066 has been calibrated against and is traceable to NBS-18 and IAEA-CO-1 (Carrara marble, $\delta^{13}C_{V-PDB}$ = + 2.5‰ and $\delta^{18}O_{V-PDB}$ = -2.4‰). NBS-18, NBS-19 and IAEA-CO-1 are inter-laboratory comparison standard materials distributed by the International Atomic Energy Agency (IAEA).

4. Results

4.1. Facies Description

On the basis of textures and depositional fabric of the carbonate rocks of the Jeribe Formation were examined to interpret the depositional environment. Microfacies analysis reveals upward grading from the lagoon (cf. laminated mudstone/wackestone), lagoonal-reefal quiet environment (cf. wackestone/

packstone) in the middle part, to agitated shoal in the upper part (cf. grainstone). The dominant microfacies are wackestone, packstone with the majority of micritized grains indicating a quite subtidal environment. Wackestone microfacies is interpreted as shallow open-marine environment and the bioclastic-packstone to grainstone microfacies indicative of deposition in relatively high energy, normal shallow marine environment (Flugel 1982). The skeletal grains comprise benthonic foraminifera, coral, corallinacea red, and calcareous algae (Table 1).

The exclusive benthic foraminifera are Soritidae, Alveolinidae and Miliolids species. The foraminiferal assemblages vary throughout the successions. The predominant species of Miliolids are *Quinquilocuilina* sp; *Austrotrilina* sp, while Soritidae species are *Peneroplis* sp. *Dendritina* sp. and Alveolinidae species just *Borelis melo* sp, with shell fragments of Mollusca (gastropod). All benthonic foraminifers' range between 0.1 and 0.5 mm.

Table 1
Main facies in the Jeribe Formation, from the older to younger.

Main Facies	Characteristics	Subdivided Microfacies	Depositional environment
Packstone	Benthic foraminifera, shell fragments and pellets	Peloidal dolomicrite packstone	Shoal Environment
Framestone	Domal Stromatolite, Densely laminated	Stromatolite Framestone	Reef Environment
Packstone	Benthic foraminifera, shell fragments and pellets	Bioclasts algae dolomicrite packstone	Open marine
Boundstone/Grainstone	Red algal and stromatolite	Coralline red algae Boundstone/Grainstone	Reef Environment
Boundstone	Coral with less algae stromatolite, and benthic foraminifera	Coral Boundstone	Reef Environment
Grainstone	Red algal with stromatolite, and benthic foraminifera	Red algal grainstone	Back reef Environment
Wackestone	Algae and less assemblage of benthic	Bioclasts dolomicrite wackestone	Open marine
Packstone	Red algae, benthic foraminifera, shell fragments and pellets	Red algae packstone	Back reef Environment
Wackestone	Algae and less assemblage of benthic	Algae dolomicrite mudstone-wackestone	Lagoon
		Pelletal Algae dolomicrite wackestone	Lagoon
Mudstone	Molluscs shell and algae	Pelletal Algae Mudstone	Lagoon
		lamination mudstone	Lagoon

4.2. CARBON-13 AND OXYGEN-18

Oxygen-18 data of the Jeribe Formation reflect several enrichment events that occurred during the middle Miocene age. Amplitude changes refer to two main zones of the enrichment after, which they get a lighter isotope. The values fluctuate between (1.62) to (2.89) in the lower part and (1.3) to (2.78) in the upper part with interval depletion to -0.97‰ values. The onset of Monterey excursion by sizable values CM1 (carbon maxima) 2.74‰, which are maximum enriched value, followed by a decline to a minimum positive value (0.05‰). Depletion values are in the middle parts caused discontinuous Monterey excursion dispute globally (Table 2).

Table 2
Analytical results of the δ ^{18}O and the δ ^{13}C

Sample No.	$^{13}C_{V-PDB}$ (‰)	$^{18}O_{V-PDB}$ (‰)	Sample	$^{13}C_{V-PDB}$ (‰)	$^{18}O_{V-PDB}$ (‰)
JA21	1.30	1.23	JB9	2.74	2.67
JA9	0.71	1.18	JB11	-0.45	1.49
JA17	-0.14	1.17	JB15	2.14	1.50
JA15	1.01	1.21	JB17	2.26	2.66
JA13	1.80	1.47	JB21	2.37	2.78
JA10	-0.87	0.12	JB27	2.14	1.75
JA9	1.07	1.62	JB31	1.65	0.99
JA6	1.59	2.80	JB37	1.31	1.22
JA1	-1.07	-0.97	JB39	0.05	0.45
JB7	2.44	2.89	JB42	-1.14	-1.15

5. Discussion

The primary isotopic signatures are readily altered during the diagenetic processes of the skeletal and non-skeletal components of the carbonate sediments (Armstrong-Altrin et al. 2011). Multiple methods have been developed to assess $\delta^{18}O$ and $\delta^{13}C$ variations during diagenetic influences involving correlation between $\delta^{18}O$ and $\delta^{13}C$ (Armstrong-Altrin et al. 2011; Oehlert and Swart 2014; Ali and Sa'ad 2018). The $\delta^{18}O$ isotope is more prone to diagenetic overprint and highly sensitive to temperature changes, especially in the bulk carbonate (Schobben et al. 2016). Therefore, a positive correlation between $\delta^{18}O$ and $\delta^{13}C$ reflects primary marine isotopic signals. As shown in Fig. 4, the stable isotopes result of the Jeribe Formation is displaying a strong correlation between $\delta^{13}C$ and $\delta^{18}O$ ($r = 0.85$). Generally, it refers to the lack of significant influence of diagenesis on the stable isotopic composition. Bivariate plots of $\delta^{18}O$ and $\delta^{13}C$ are another convenient method. It is used to distinguish the depositional and/or diagenetic environments of carbonate rocks. (Hudson 1977; Nelson and Smith 1996) had used a $\delta^{18}O$ and $\delta^{13}C$ cross-plot to identify the origins of different types of carbonate rocks. Therefore, this approach has been adopted by many workers, such as (Bathurst 1983; Choquette and James 1987; Moore 1989; Morse and Mackenzie 1990). Despite significant effaces of evaporation, meteoric dilution, and carbon transfer in the shallow marine relative to platform margin, slope, and basinal environments, the isotopes composition in the investigated succession exhibits primary stable isotope values and can be used as a direct proxy for the composition of seawater in the Kirkuk- Dezful Embayment during the Middle Miocene (Figs. 4 and 5).

Carbonates of the Jeribe Formation show vertical variation in $\delta^{18}O$ and $\delta^{13}C$ composition; however, most samples have positive values. At the bottom of the succession, the boundary of the Early-Middle Miocene is marked by prominent negative values of the $\delta^{18}O$ and $\delta^{13}C$. However, both isotopes display enrichment after depletion, which is marking the beginning of transgression in the Middle Miocene, denotate Ng30 date of the final closure of Neo-Tethys by (Sharland et al. 2004). Enrichment of both $\delta^{13}C$ and $\delta^{18}O$ isotopes has occurred in two main zones. It is separated by depletion in the middle unit, on both of the $\delta^{13}C$ and $\delta^{18}O$. It is clearly expressed by a vertical change in the environmental conditions from the lagoon to the reef environment and shoal facies in the uppermost at the contact with the overlying Fatha Formation.

Mi zones have been identified and defined using the criteria of Miller, Wright, et al. (1991) based on the maximum $\delta^{18}O$ value. The current study represents a single-point zone recorded with more details about Mi2, Mi3, zones, where Mi3 has been subdivided into Mi2b, Mi2c, and Mi2d, while Mi3 zone is subdivided into Mi3a, Mi3b, and Mi3c. These discernible deviations represent a minor step in the major cooling trend started with Mi 3 and Mi2, that gradual increase in glaciation has a profound and immediate impact on the depositional environment of the Jeribe Formation.

Coralline algae are used to assess the paleo-climate, paleo-latitudes, and paleo-depth (Mccoy and Kamenos, 2015). They have wide temperature range tolerate and live at depths of 125 m or more in moderate wave energy areas (Scholle and Ulmer-Scholle 2003). They are sensitive to water depth and terrigenous input. Corallines, in general, prefer decreased siliciclastic loading and shallow to mildly deeper bathymetric (Sarkar et al. 2016). Coralline red algae of the corallinales order (Archaeolithothamnium, sp and Mesophyllum, sp) are identified as autochthonous form. They comprise the major type in the middle part of the Jeribe Formation associated with coral and benthic foraminifera.

Dasycladaceae is one of the large calcareous green algae families, which are not abundant in the Jeribe Formation. The green and the red algae are observed in the onset of the middle unit of the studied sections. Dasycladaceae green algae commonly occur in quiet, shallow, or very shallow, normal salinity, and warm water in the reef-lagoon environment (Flugel and Flügel, 2004). This environment is characterized by abundant green algae at depths of 50–100 m in the reef and near-back reef areas. It is more significant of modern and ancient carbonate deposits of warm water regions (Scholle and Ulmer-Scholle 2003). Green algae are mostly indicative of back reef-lagoon facies. The distribution of small encrusting green and red algae can be used to estimate the depth-related zones (Flügel 2012).

The presence of red and green algae together indicates that the sedimentation had occurred in the upper part of the photic zone. The absence of green algae in the lower part within the lagoonal environments and the middle part within the coral reef facies reflect cold water relatively; while the uppermost part within the shoal facies reflects high energy. They observed together within the back-reef to reef facies.

The recognized coral occurs in the middle part of the successions. It represents tropical environments, normal salinity, and waters at depths from the intertidal zone to a few tens of meters. It is mainly in areas

with a relatively low influx of terrigenous sediments (Scholle and Ulmer-Scholle 2003). Corals contributed significantly to the formation of large and extended reef-structures in the deeper- and cold-water settings. However, it is also in relatively shallow warm-temperate environments (Flugel and Flügel 2004). Corals that occur in situ were found in a shelf sequence formed during a relatively sea-level highstand (Scholle and Ulmer-Scholle 2003). Observed coral reefs and the absence of green algae indicated sea level rise and/or subsidence occurrences. In cause subsidence's occurrence that relevant for brecciate outcropping, indicate changes in nutrient supply are regarded as a major control on productivity. Slumping and sliding are controlled and triggered by high rates of sedimentation creating oversteep slopes and differential compaction (Flugel and Flügel 2004).

In the upper part, the red algae, stromatolites, and benthic foraminifera are identified. Corallinacean algae and abundant foraminiferal types reflect the shallow open marine environments (Flügel 2012). Red algae and the benthic foraminifera emphasize deposition in the upper photic zone to the upper part of the lower photic zone. Stromatolites were observed in the upper part of the succession within reef environments. It represents the range from subtidal to intertidal settings (Scholle and Ulmer-Scholle 2003). They are commonly set in tidal and subtidal carbonates as well as in subtidal shelf carbonates or shallow subtidal environments. They take their energy from the decomposition of organic material to inorganic components by redox processes in shallow-water settings (Flugel and Flügel, 2004).

In the lagoonal environments, mudstone facies exhibit the lowest values on both $\delta^{13}C$ and $\delta^{18}O$, while wackestone facies display shifts towards high values. (CM 1) the event formed over wackestone facies, that occurrences as the interval between two major cooling Mi 2a and Mi 2b. Suggests the differentiation between the mudstone and wackestone facies due to different depositional energy, which appears to be the major controlling factor to the heaviest and linked to glacial-eustatic.

High energy in packstone and grainstone facies within the back reef environments display depleted on $\delta^{13}C$ within major glacial zones Mi 2b and Mi 2c. Enrichment by $\delta^{18}O$ and absences of green algae indicative glacially climate. According to (Purkis et al. 2015), grainstone and boundstone facies are indicative of water depths < 5 m while wackestone at depths of > 20 m. Suggests sea-level fall in this interval caused to the glacial event. In shallow open marine, moderately energy represent by wackestone facies amongst back reef environments exhibit highest values of ^{13}C and formed (CM 2), associated with miner step in the major cooling. Hasenclever et al. (2017) suggests that growing ice-sheets as a result of reduced volcanic emissions have been affected on the global decrease in sea level. Glacio-eustatic sea-level rose has been controlling on facies change.

Reef facies showed substantial variation in the $\delta^{13}C$ and $\delta^{18}O$ associated with a change in skeletal grain. Reef environments represent by boundestone and framestone facies display the highest values on both the $\delta^{13}C$ and $\delta^{18}O$ and formed CM 3 to 6 events, synchronous with major glacial zones Mi 3a, b, and c. Shifted to depletion on the ^{13}C and ^{18}O value at the onset of the reef facies with significant differences in the types of the skeletal grain to coral mat compared to other fossils. Coral reefs are important proxy data due to their sensitivity to temperature. It's affected by cooling episodes that prevented coral reef growth.

This shifted to depletion reflected short-term inter-glacial events. According to Immenhauser et al. (2002), restricted-platform water displays relatively low ^{13}C values due to remineralized organic carbon during the long residence time of seawater on the platform. Breccia records in these facies emphases tectonic event may be uplift with the shallowest setting occurrence, reflects oceanographic changes.

These events coupled to short-term events records indicated by depleted in ^{18}O relatively near 0‰ and display the more negative value in ^{13}C as interval events between CM 3 and 4 and CM 5 and 6, suggesting interglacial periods and oceanographic changes within reef environments.

Relatively high energy in the packstone facies within the second cycle of shallow open marine shows, relatively, lowest values in ^{13}C. Continual enhancing of the ^{18}O values by upwelling at this facies reflect cooling of the surface waters; while decreases of the $\delta^{13}C$ values, reflect variations in carbonate production and accumulation rates, because the carbonate production is lower in the cool water, suggesting this period as minor step of major cooling. High energy in the garinstone facies of the shoal environments display more negative on both ^{13}C and ^{18}O value. Shoaling reflects climatic and oceanographic changes that impacted the integral closure of the Tethys seaway during the middle Miocene.

On these bases, the variability of ^{13}C came from depositional energy in the shallowest setting that linked to glacial-eustatic within Mi 2 zone, as interglacial periods indicated by coincidentally with high carbonate production. According to the Grossman (2008), sea level falls, as continental ice sheets and glaciers expand is a primary force that influences reef initiation, development and enabling coral-reef animals, and plants to settle and growth. Mi 3 zone is controlled by Glacio-eustatic sea-level fall. Local tectonic events indicated by breccia records at the onset of Mi 3 zone reflects oceanographic changes, association with coral reef growth indicates major climatic changes into the greenhouse as a short term.

According to Mason, Edmonds, and Turchyn (2017), carbon is originated from volcanic arc, represent an essential source in the marine environment. Subduction-related volcanic arcs, particularly, continental arcs, are the main source of heavier carbone due to reworking of crustal limestone that is often associated with the closing of ocean basins. Weissert and Erba (2004) mentioned that the major positive C-isotope anomalies in the Early Cretaceous coincide with episodes of volcanic activity. Moreover, Volcanic arc occurred during the thrusting and later closing of the ocean, is combined with increased ^{13}C, suggests high $\delta^{13}C$ concentration as CM-events in shallow marine carbonates linked to the structural location of Kirkuk- Dezful Embayment, which is lying adjacent to the volcanic activity and coincide to the platform destruction during the final phase of Tethys sea closure. Many published papers are mentioned to the Mi 3b Mi 3b is marking the final major cooling step and ended of the Monterey Excursion (Miller et al. 1991a; Zachos et al. 2001, 2008a; Shevenell et al. 2004, 2008). In the current study, Mi 3c marking final major cooling coincide with the ended of the Monterey Excursion (Fig. 6).

6. Conclusion

This study focused on identifying the facies of the Jeribe Formation and stable isotopes. This formation is deposited during the final face of the Tethys sea closure (Middle Miocene age) as a shallow marine deposition on the Arabian plate.

Mi zones have been identified based on the maximum $\delta^{18}O$ value. Middle Miocene in the shallowest marine has Mi 2, Mi 3, and Mi 3a zones with additional details about Mi 2 and Mi 3 zones. The Mi 3 has a minor step in the major cooling represented by Mi 3a, Mi 3b, and Mi 3c, Mi 2 zone also is subdivided into three minor steps, which are Mi 2a, Mi 2b, and Mi 2c. These deviations denote Mi zones represent cool water by increase upwelling current and prominent facies changes occur synchronously with CM-event, subsequently with high rates of sedimentation. The positive value of the ^{13}C (CM-events) is controlled by proximity to the depositional energy and tectonic activities, which can bury carbonate-producing organisms and enhancing ^{13}C. The peaks of heavy ^{13}C represents polyphase deformation and platform destruction in the subduction zone on the north-eastern margin of the Arabian plate.

Declarations

Author Contributions

Mustafa A. Ali did the following: conceptualization, data curation, formal analysis, and investigation. Sa'ad Z. Al-Mashaikie and Arsalan Ahmed Othman did the following: reviewing and editing.

References

1. Ali MA, Sa'ad Z (2018) **Application of 18O and 13C stable isotopes composition of the carnonate rocks of the Jeribe Formation Eastern Iraq; an approach to define the plaeo temperature and paleo depth**. Iraqi Geol J **83–100**
2. Amodio S, Ferreri V, D'Argenio B, **et al (** (2008) Carbon-isotope stratigraphy and cyclostratigraphy of shallow-marine carbonates: the case of San Lorenzello, Lower Cretaceous of southern Italy. Cretac Res 29:803–813. https://doi.org/10.1016/j.cretres.2008.05.022 **)**
3. Aqrawi AAM, Mahdi TA, Sherwani GH, Horbury AD (2010) **Characterization of the mid-Cretaceous Mishrif reservoir of the southern Mesopotamian basin, Iraq. In: American Association of Petroleum Geologists Conference and Exhibition. pp 7–10**
4. Armstrong-Altrin JS, Lee YI, Verma SP, Worden RH (2009) Carbon, oxygen, and strontium isotope geochemistry of carbonate rocks of the upper Miocene Kudankulam Formation, southern India: Implications for paleoenvironment and diagenesis. Chem Erde 69:45–60. https://doi.org/10.1016/j.chemer.2008.09.002 **()**
5. Armstrong-Altrin JS, Madhavaraju J, Sial AN, **et al (** (2011) Petrography and stable isotope geochemistry of the cretaceous El Abra Limestones (Actopan), Mexico: Implication on diagenesis. J Geol Soc India 77:349–359 **)**

6. Auer G, Piller WE, Reuter M, Harzhauser M (2015) Correlating carbon and oxygen isotope events in early to middle Miocene shallow marine carbonates in the Mediterranean region using orbitally tuned chemostratigraphy and lithostratigraphy. Paleoceanography 30:332–352. https://doi.org/10.1002/2014PA002716 ()
7. Bathurst RGC (1983) **Early diagenesis of carbonate sediments**. **In**: **Sediment Diagenesis**. **Springer**, **pp 349–377**
8. Bellen RCv, Dunnington HV, Wetzel R, Morton D (1959) Lexique Stratigraphic International. Asie, Fasc, Iraq, **Paris** ()
9. Billups K, Schrag DP (2003) Application of benthic foraminiferal Mg/Ca ratios to questions of Cenozoic climate change. Earth Planet Sci Lett 209:181–195. https://doi.org/10.1016/S0012-821X(03)00067-0 ()
10. Chakrabarti G, Shome D, Kumar S, **et al** ((2011) Carbon and oxygen isotopic variations in stromatolitic dolomites of Palaeoproterozoic Vempalle Formation, Cuddapah Basin, India. Carbonates Evaporites 26:181–191)
11. Chaproniere GCH (1981) Late Oligocene to early Miocene planktic Foraminiferida from Ashmore Reef No. 1 Well, northwest Australia. Alcheringa 5:103–131 ()
12. Choquette PW, James NP (1987) **Diagenesis# 12**. **Diagenesis in Limestones-3**. **The deep burial environment**. **Geosci Canada**
13. Cooke PJ, Nelson CS, Crundwell MP (2008) Miocene isotope zones, paleotemperatures, and carbon maxima events at intermediate water-depth, Site 593, Southwest Pacific. New Zeal J Geol Geophys 51:1–22 ()
14. Coplen TB, Kendall C, Hopple J (1983) Comparison of stable isotope reference samples. Nature 302:236–238 ()
15. Corfield RM, Cartlidge JE (1993) **Oxygen and carbon isotope stratigraphy of the middle Miocene**, **Holes 805B and 806B**. **In**: **Proceedings of the Ocean Drilling Program**. **Scientific Results**. **pp 307–322**
16. Diester-Haass L, Billups K, Jacquemin I, **et al** ((2013) Paleoproductivity during the middle Miocene carbon isotope events: A data-model approach. Paleoceanography 28:334–346)
17. Edgar KM, Anagnostou E, Pearson PN, Foster GL (2015) Assessing the impact of diagenesis on δ11B, δ13C, δ18O, Sr/Ca and B/Ca values in fossil planktic foraminiferal calcite. Geochim Cosmochim Acta 166:189–209 ()
18. Flower BP, Kennett JP (1993) **Relations between Monterey Formation deposition and Middle Miocene global cooling: Naples Beach section, California**. Geology **21**:**877–880**. https://doi.org/10.1130/0091-7613(1993)021<0877:RBMFDA>2.3.CO;2
19. Flower BP, Kennett JP (1994) The middle Miocene climatic transition: East Antarctic ice sheet development, deep ocean circulation and global carbon cycling. Palaeogeogr Palaeoclimatol Palaeoecol 108:537–555 ()
20. Flower BP, Kennett JP (1995) Middle Miocene deepwater paleoceanography in the southwest Pacific: relations with East Antarctic Ice Sheet development. Paleoceanography 10:1095–1112 ()

21. Flugel E (1982) **Microfacies analysis of limestones**
22. Flügel E (2012) **Microfacies analysis of limestones**. **Springer Science** & **Business Media**
23. Flugel E, Flügel E (2004) **Microfacies of carbonate rocks**: **analysis**, **interpretation and application**. **Springer Science** & **Business Media**
24. Fouad SFA (2012) **Western Zagros Fold–Thrust Belt, Part I: The Low Folded Zone**. Iraqi Bull Geol Min **39–62**
25. Gröcke DR, Price GD, Robinson SA, **et al (** (2005) The Upper Valanginian (Early Cretaceous) positive carbon–isotope event recorded in terrestrial plants. Earth Planet Sci Lett 240:495–509)
26. Grossman EE (2008) Sea level and its effects on reefs in Hawai'i. US Geol Surv Sci Investig Rep 2007–5101:101–104 ()
27. Hasenclever J, Knorr G, Rüpke LH, **et al (** (2017) Sea level fall during glaciation stabilized atmospheric CO 2 by enhanced volcanic degassing. Nat Commun 8:1–11)
28. Holbourn A, Kuhnt W, Schulz M, **et al (** (2007) Orbitally-paced climate evolution during the middle Miocene "Monterey" carbon-isotope excursion. Earth Planet Sci Lett 261:534–550. https://doi.org/10.1016/j.epsl.2007.07.026)
29. Hudson JD (1977) Stable isotopes and limestone lithification. J Geol Soc London 133:637–660 ()
30. Immenhauser A, Kenter JAM, Ganssen G, **et al (** (2002) Origin and significance of isotope shifts in Pennsylvanian carbonates (Asturias, NW Spain). J Sediment Res 72:82–94)
31. Jassim SZ, Goff JC (2006) **Geology of Iraq**. **Dolin**, **prague and moravian museum**. **Brno**, **2006**–**341 pp**
32. Kumar B, Das Sharma S, Sreenivas B, **et al (** (2002) Carbon, oxygen and strontium isotope geochemistry of Proterozoic carbonate rocks of the Vindhyan Basin, central India. Precambrian Res 113:43–63. https://doi.org/10.1016/S0301-9268(01)00199-1)
33. Madhavaraju J, Kolosov I, Buhlak D, **et al (** (2004) Carbon and oxygen isotopic signatures in Albian-Danian limestones of Cauvery Basin, southeastern India. Gondwana Res 7:519–529. https://doi.org/10.1016/S1342-937X(05)70802-9)
34. Maheshwari A, Sial AN, Guhey R, Ferreira VP (2005) C-isotope composition of carbonates from Indravati Basin, India: Implications for regional stratigraphic correlation. Gondwana Res 8:603–610. https://doi.org/10.1016/S1342-937X(05)71161-8 ()
35. Marquillas R, Sabino I, Nobrega Sial A, **et al (** (2007) Carbon and oxygen isotopes of Maastrichtian-Danian shallow marine carbonates: Yacoraite Formation, northwestern Argentina. J South Am Earth Sci 23:304–320. https://doi.org/10.1016/j.jsames.2007.02.009)
36. Mason E, Edmonds M, Turchyn AV (2017) Remobilization of crustal carbon may dominate volcanic arc emissions. Science 357:290–294 ()
37. Miller KG, Feigenson MD, Wright JD, Clement BM (1991a) Miocene isotope reference section, Deep Sea Drilling Project Site 608: an evaluation of isotope and biostratigraphic resolution. Paleoceanography 6:33–52 ()

38. Miller KG, Katz ME (1987) Oligocene to Miocene benthic foraminiferal and abyssal circulation changes in the North Atlantic. Micropaleontology 33:97–149 ()
39. Miller KG, Wright JD, Fairbanks RG (1991b) Unlocking the ice house: Oligocene-Miocene oxygen isotopes, eustasy, and margin erosion. J Geophys Res Solid Earth 96:6829–6848 ()
40. Moore CH (1989) **Carbonate diagenesis and porosity**. **Elsevier**
41. Morse JW, Mackenzie FT (1990) **Geochemistry of sedimentary carbonates**. **Elsevier**
42. Mourik AA, Bijkerk JF, Cascella A, **et al (** (2010) Astronomical tuning of the La Vedova High Cliff section (Ancona, Italy)-Implications of the Middle Miocene Climate Transition for Mediterranean sapropel formation. Earth Planet Sci Lett 297:249–261. https://doi.org/10.1016/j.epsl.2010.06.026)
43. Nagarajan R, Sial AN, Armstrong-Altrin JS, **et al (** (2008) Carbon and oxygen isotope geochemistry of Neoproterozoic limestones of the Shahabad Formation, Bhima basin, Karnataka, southern India. Rev Mex Ciencias Geológicas 25:225–235)
44. Nelson CS, Smith AM (1996) Stable oxygen and carbon isotope compositional fields for skeletal and diagenetic components in New Zealand Cenozoic nontropical carbonate sediments and limestones: a synthesis and review. New Zeal J Geol Geophys 39:93–107. https://doi.org/10.1080/00288306.1996.9514697 ()
45. Numan N (1997) A plate tectonic scenario for the Phanerozoic succession in Iraq. Iraqi Geol J 30:85–119 ()
46. Oehlert AM, Swart PK (2014) Interpreting carbonate and organic carbon isotope covariance in the sedimentary record. Nat Commun 5:1–7 ()
47. Purkis SJ, Rowlands GP, Kerr JM (2015) Unravelling the influence of water depth and wave energy on the facies diversity of shelf carbonates. Sedimentology 62:541–565 ()
48. Raymo ME, Ruddiman WF, Froelich PN (1988) Influence of late Cenozoic mountain building on ocean geochemical cycles. Geology 16:649–653 ()
49. Rea DK, Snoeckx I, Joseph LH (1998) Late Cenozoic Eolian deposition in the North Pacific: Asian drying, Tibetan uplift, and cooling of the northern hemisphere. Paleoceanography 13:215–224. https://doi.org/10.1029/98PA00123 ()
50. Ruddiman WF, Raymo ME, Prell WL, Kutzbach JE (1997) **The uplift-climate connection**: **a synthesis**. **In**: **Tectonic uplift and climate change**. **Springer**, **pp 471–515**
51. Sarkar S, Ghosh AK, Rao GMN (2016) Coralline algae and benthic foraminifera from the long formation (middle Miocene) of the Little Andaman Island, India: Biofacies analysis, systematics and palaeoenvironmental implications. J Geol Soc India 87:69–84 ()
52. Schobben M, Ullmann CV, Leda L, **et al (** (2016) Discerning primary versus diagenetic signals in carbonate carbon and oxygen isotope records: An example from the Permian–Triassic boundary of Iran. Chem Geol 422:94–107)
53. Scholle PA, Arthur MA (1980) Carbon isotope fluctuations in Cretaceous pelagic limestones: potential stratigraphic and petroleum exploration tool. Am Assoc Pet Geol Bull 64:67–87 ()

54. Scholle PA, Ulmer-Scholle DS (2003) **A Color Guide to the Petrography of Carbonate Rocks**: **Grains**, **Textures**, **Porosity**, **Diagenesis**, **AAPG Memoir 77**. **AAPG**
55. Scott GH, Nelson CS, Stone HH (1995) Planktic foraminiferal events in early Miocene Zones N.6 and N.7 at southwest Pacific DSDP Site 593: relation with climatic changes in oxygen isotope Zone Milb. Mar Micropaleontol 25:29–45. https://doi.org/10.1016/0377-8398(94)00025-I ()
56. Sharland PR, Casey DM, Davies RB, **et al (** (2004) Arabian plate sequence stratigraphy–revisions to SP2. GeoArabia 9:199–214)
57. Shevenell AE, Kennett JP, Lea DW (2008) Middle Miocene ice sheet dynamics, deep-sea temperatures, and carbon cycling: A Southern Ocean perspective. Geochemistry Geophys Geosystems 9:. https://doi.org/10.1029/2007GC001736
58. Shevenell AE, Kennett JP, Lea DW (2004) Middle Miocene southern ocean cooling and Antarctic cryosphere expansion. Science 305:1766–1770. https://doi.org/10.1126/science.1100061 ()
59. Smart CW, Murray JW (1994) An early Miocene Atlantic-wide foraminiferal/palaeoceanographic event. Palaeogeogr Palaeoclimatol Palaeoecol 108:139–148. https://doi.org/10.1016/0031-0182(94)90026-4 ()
60. Sosdian SM, Babila TL, Greenop R, **et al (** (2020) Ocean Carbon Storage across the middle Miocene: a new interpretation for the Monterey Event. Nat Commun 11:1–11)
61. Vincent E, Berger WH (1985) Carbon dioxide and polar cooling in the Miocene: The Monterey hypothesis. carbon cycle Atmos CO2 Nat Var Archean to Present 32:455–468 ()
62. Weissert H, Erba E (2004) Volcanism, CO2 and palaeoclimate: a Late Jurassic–Early Cretaceous carbon and oxygen isotope record. J Geol Soc London 161:695–702 ()
63. Westerhold T, Bickert T, Röhl U (2005) Middle to late Miocene oxygen isotope stratigraphy of ODP site 1085 (SE Atlantic): new constrains on Miocene climate variability and sea-level fluctuations. Palaeogeogr Palaeoclimatol Palaeoecol 217:205–222 ()
64. Woodruff F, Savin S (1991) Mid-Miocene isotope stratigraphy in the deep sea: High-resolution correlations, paleoclimatic cycles, and sediment preservation. Paleoceanography 6:755–806. https://doi.org/10.1029/91PA02561 ()
65. Wright JD, Miller KG, Fairbanks RG (1992) Early and Middle Miocene stable isotopes: Implications for Deepwater circulation and climate. Paleoceanography 7:357–389. https://doi.org/10.1029/92PA00760 ()
66. Zachos J, Pagani M, Sloan L, **et al (** (2001) Trends, rhythms, and aberrations in global climate 65 Ma to present. Science 292:686–693)
67. Zachos JC, Dickens GR, Zeebe RE (2008a) An early Cenozoic perspective on greenhouse warming and carbon-cycle dynamics. Nature 451:279–283. https://doi.org/10.1038/nature06588 ()
68. Zachos JC, Dickens GR, Zeebe RE (2008b) An early Cenozoic perspective on greenhouse warming and carbon-cycle dynamics. Nature 451:279–283. https://doi.org/10.1038/nature06588 ()

Figures

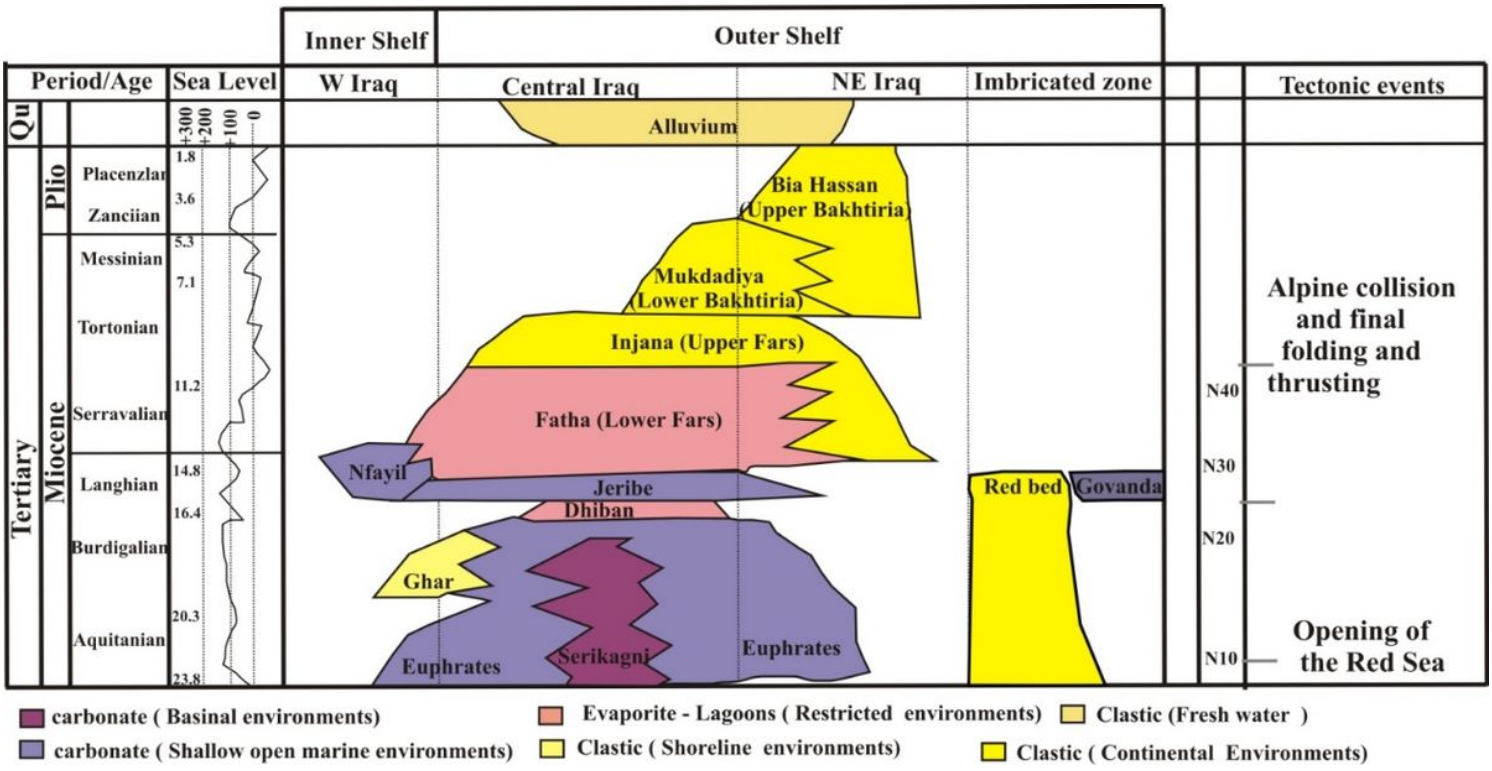

Figure 1

Stratigraphic column shows the Miocene epoch (modified after Jassim and Goff, 2006).

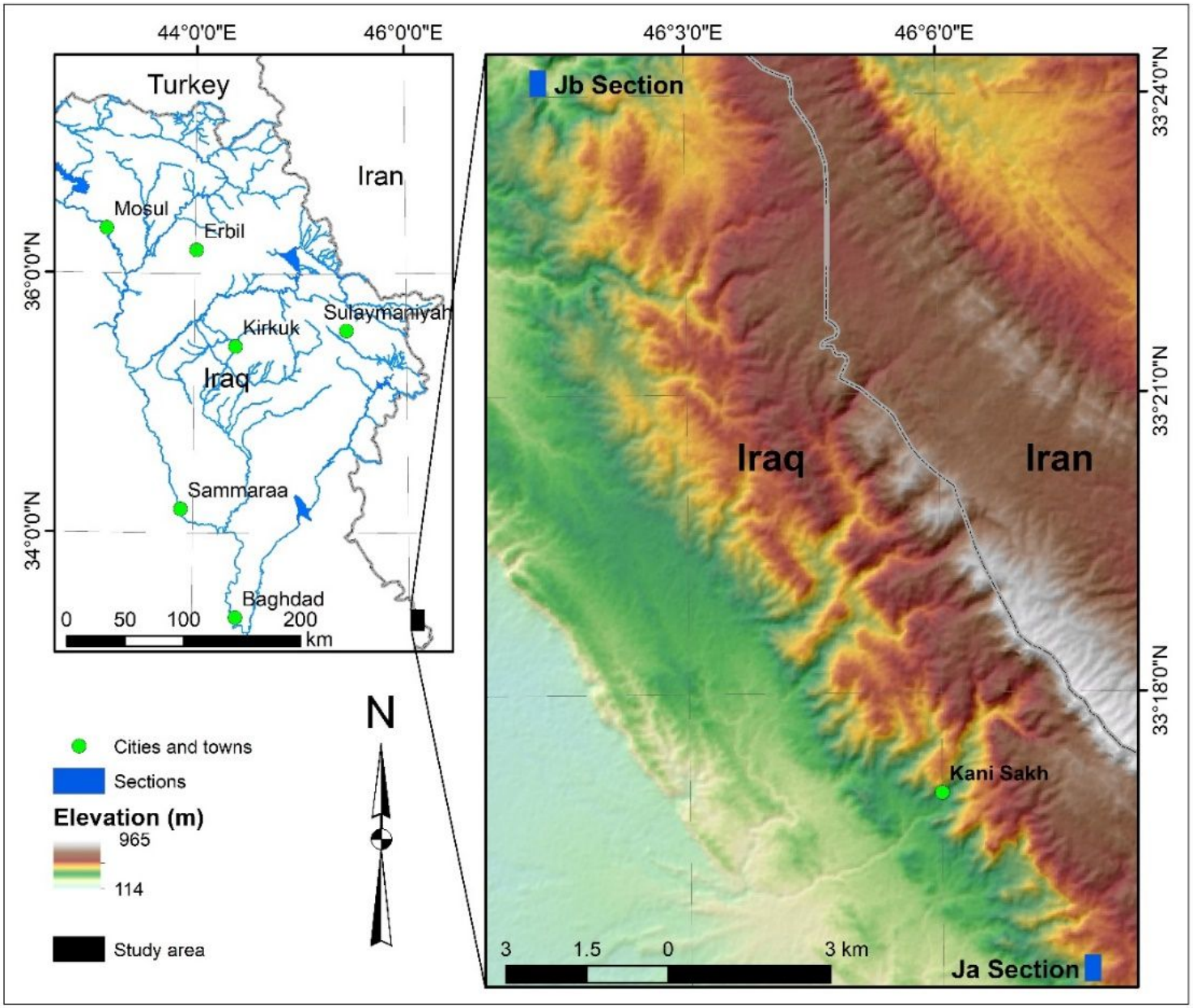

Figure 2

Map showing the location of the Ja and the Jb sections. Note: The designations employed and the presentation of the material on this map do not imply the expression of any opinion whatsoever on the part of Research Square concerning the legal status of any country, territory, city or area or of its authorities, or concerning the delimitation of its frontiers or boundaries. This map has been provided by the authors.

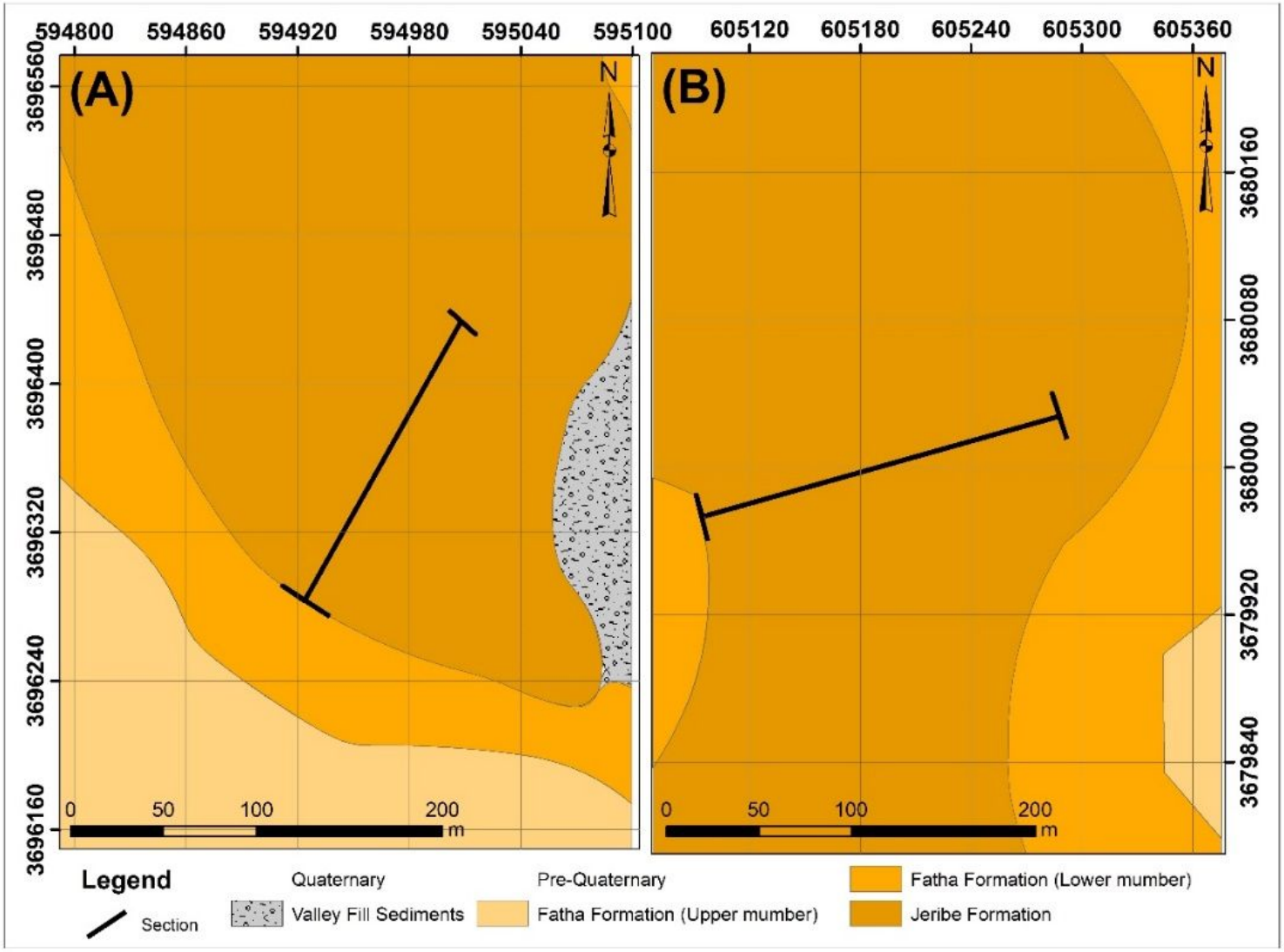

Figure 3

Geological maps of the study area, showing the selected stratigraphic sections of (A) Jb and (B) Ja area.

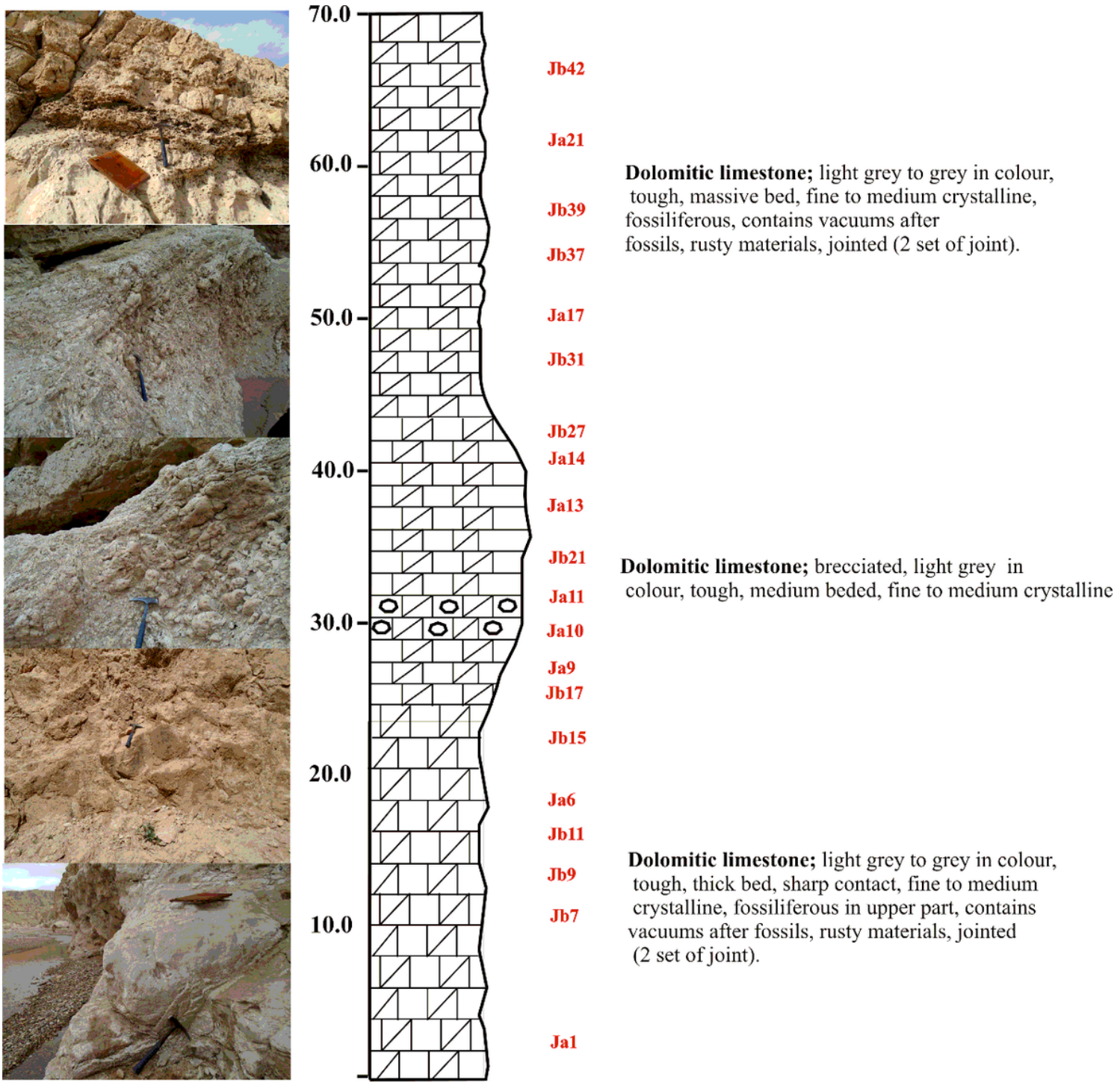

Figure 4

Ideal composite column from selected stratigraphic sections, shows vertical distribution of the selected samples based on the well-preserved texture.

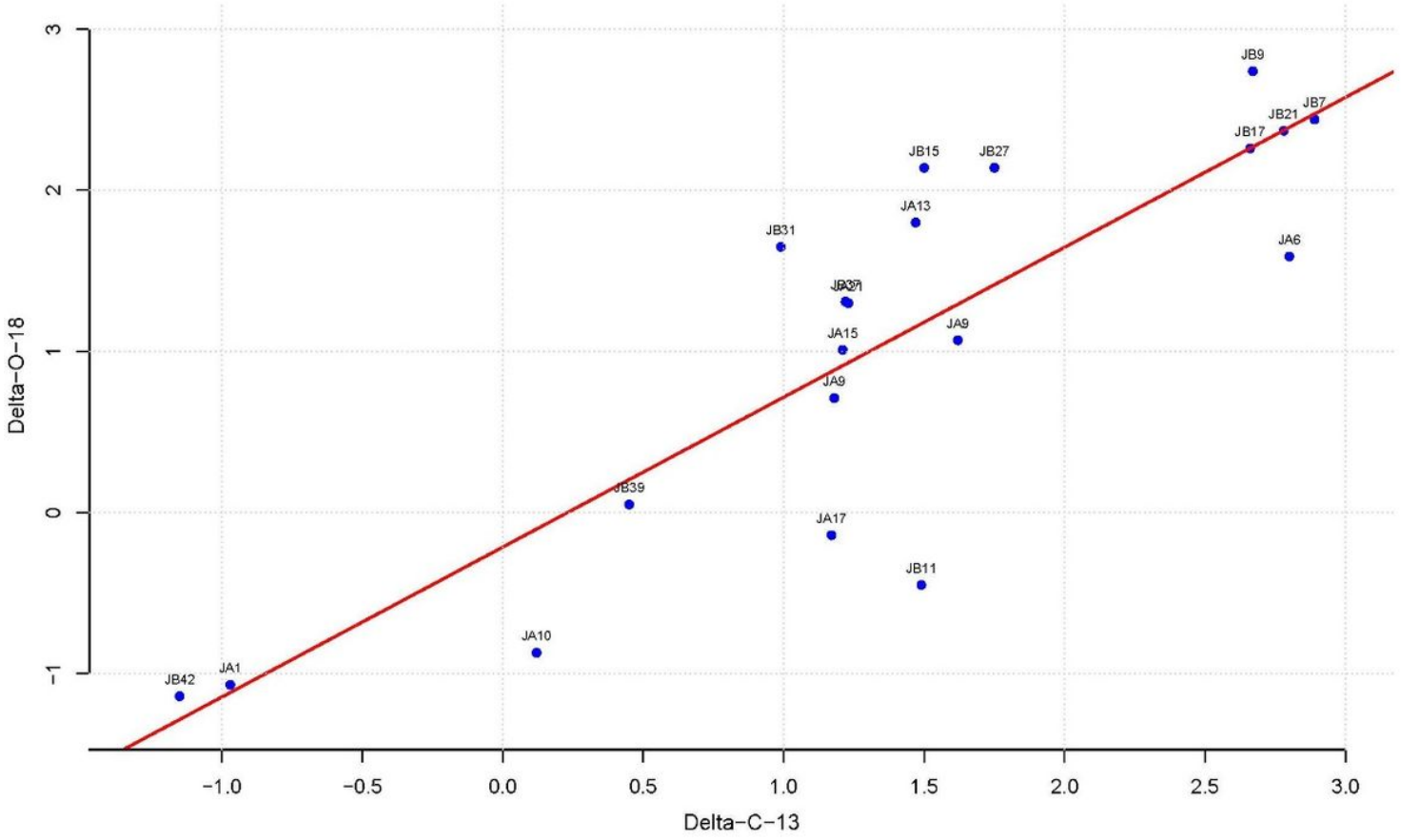

Figure 5

Correlation between the δ13C and the δ18O

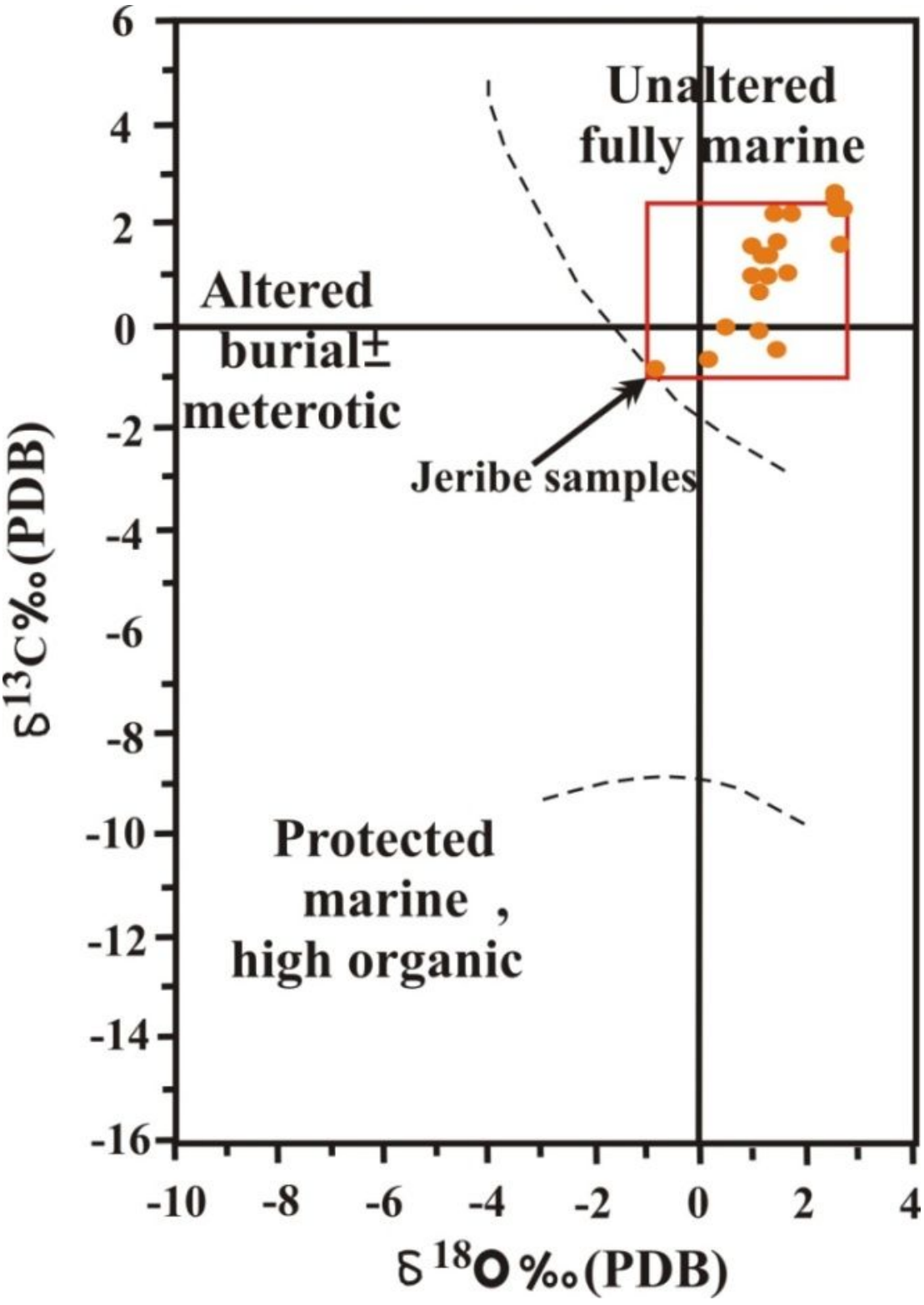

Figure 6

δ18O and δ13C plots from the Jeribe Formation showing primary signature of isotopes

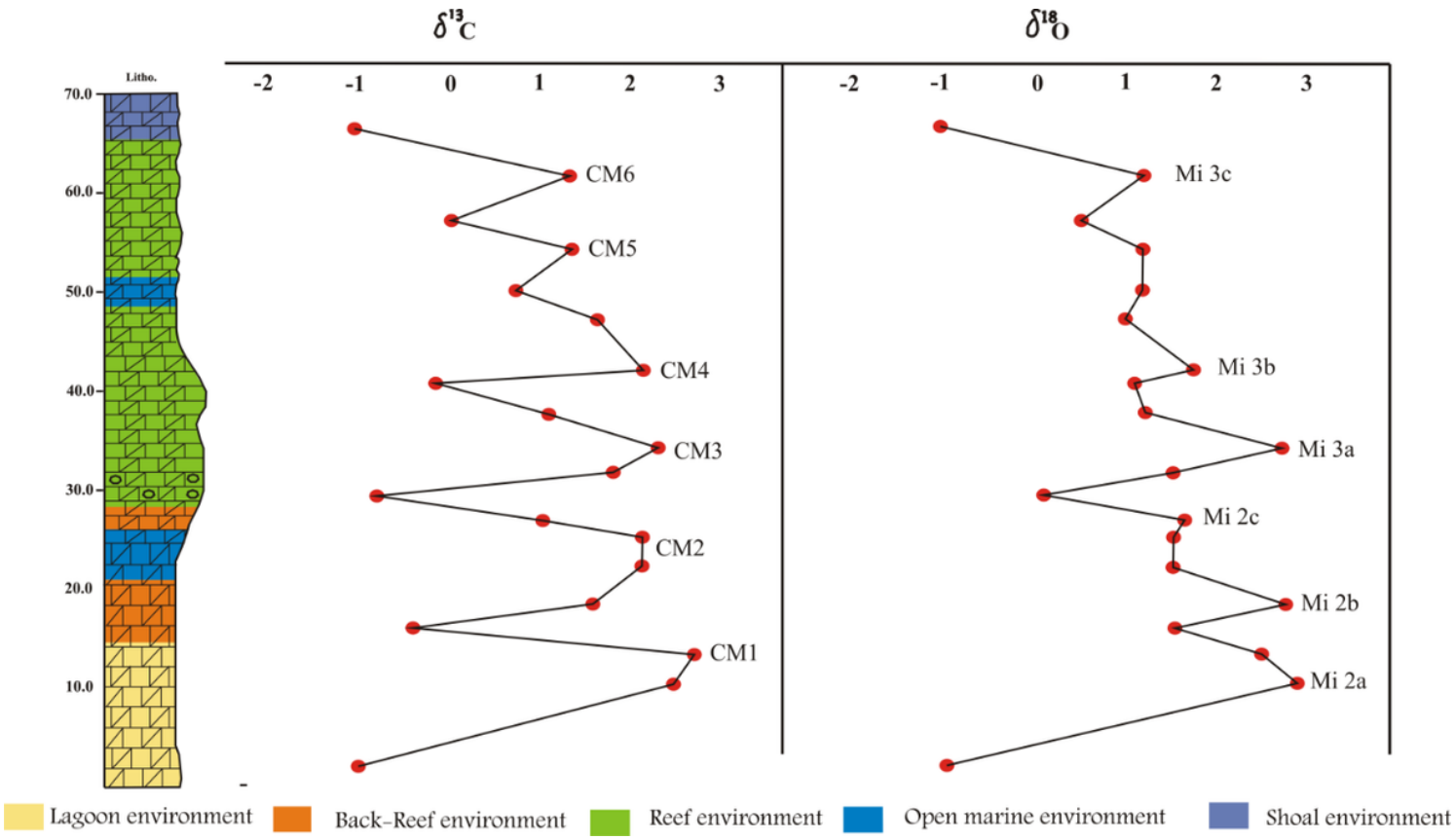

Figure 7

Stable isotopes distribution in the Jeribe succession.